Available online at www.sciencedirect.com
ScienceDirect
Combustion and Flame 153 (2008) 384–393
Combustion and Flame
www.elsevier.com/locate/combustflame

How "flat" is the rich premixed flame produced by your McKenna burner?

F. Migliorini, S. De Iuliis *, F. Cignoli, G. Zizak

CNR-IENI, Istituto per l'Energetica e le Interfasi, Sez. di Milano, via Cozzi 53, 20125 Milan, Italy

Received 30 March 2007; received in revised form 9 October 2007; accepted 10 January 2008

Available online 5 March 2008

Abstract

McKenna burners are widely used in the combustion community for producing "flat" premixed flames. These flames are considered as standards for the development and calibration of optical techniques. Rich premixed flames produced by McKenna burners are frequently investigated in order to understand soot formation processes both by optical and by sampling techniques. Measurements are normally performed along the axis of the flames, with a uniform distribution of temperature and species concentration assumed in the radial direction. In this work it is shown that the soot radial profiles of rich premixed ethylene–air flames produced by a McKenna burner with a stainless steel porous plug may be far from being "flat." Soot is mainly distributed in an annular region and nonsoot fluorescing species are present in the core of the flames. This surprising result was verified under several working conditions. Furthermore, flames cannot be considered axial-symmetric but present a skewed soot distribution. Another McKenna burner with a bronze porous disk was used to produce flames of the same equivalence ratio and flows. These flames show a completely different soot radial profile, closer to the claimed flat distribution. These results cast doubts about the conclusions drawn in several studies on soot formation performed with a stainless steel McKenna burner.

Keywords: McKenna burner; Rich premixed flames; Soot; Optical diagnostics

1. Introduction

McKenna burners have been widely used for many years to produce flat premixed flames [1]. The flame is assumed to be one-dimensional and considered as a standard, at least under lean and close-to-stoichiometric conditions. The burner is employed in many laboratories around the world for the development and calibration of optical diagnostic techniques [2–6]. Coherent anti-Stokes Raman scattering measurements have been performed by Prucker and co-workers on H_2/air flames in order to determine temperatures for many stoichiometries (from 0.5 to 1.3), flow rates, and heights above the burner [7]. The corresponding exhaust gas composition has been derived from equilibrium calculations. Moreover, spatial uniformity in the flame radial direction is also claimed. Recently, a high-accuracy Rayleigh scattering thermometry system has been used by Sutton et al. to calibrate a premixed flat-flame burner with an equivalence ratio of 0.8–1.5 [8]. Measurements were performed on a propane/air flame, but, as the authors observed, similar results could be obtained with any

* Corresponding author. Fax: +39 02 66173321.
E-mail address: s.deiuliis@ieni.cnr.it (S. De Iuliis).

0010-2180/$ – see front matter
doi:10.1016/j.combustflame.2008.01.007

fuel and oxidizer. In such work it has been verified that the burner and the associated gas mixing system can be considered as a standard for combustion temperature and species.

Several works, reported in the literature, are also performed under rich conditions, devoted to the study of the mechanisms responsible for soot formation, and consequently to the investigation of both gas species and nanoparticles. As reported by many authors, measurements performed by using several optical and sampling techniques result to be very helpful for the implementation and validation of chemical kinetics codes [9–15]. In particular, the McKenna burner was recently proposed and utilized as a standard burner for the development of the laser-induced incandescence (LII) technique [16–18].

Different models of this burner are commercially available, with either a stainless steel or a bronze porous disk. In the literature, not all authors report detailed and complete information about their experimental conditions. For example, few specifications are usually given by authors about the utilization of the nitrogen shroud, which makes it possible to avoid the air entrainment responsible for the formation of an external diffusion flame.

During an investigation of the influence of a sampling probe on soot distribution in rich premixed flames from a McKenna burner, we observed a hollow soot distribution. Puzzled by this finding, we tested several burners: two brand new ones made of stainless steel but, according to the manufacturer, produced by different pressing machines, a used one made of stainless steel, and belonging to a different research group, and a new one made of bronze. For all the burners made of stainless steel, a hollow soot distribution was found, while a nearly "flat" distribution was observed for the burner made of bronze. In this work, the results of our investigation of soot distribution in rich ethylene/air premixed flames produced with the two models (i.e., steel and bronze) of the burner are presented. Scattering line imaging and laser-induced incandescence (LII) are employed to analyze soot distribution in such flames. Moreover, to distinguish the contribution from soot nanoparticles from that coming from different "nonsolid" species, laser-induced fluorescence measurements are also carried out. Extinction and scattering line-imaging measurements are performed to investigate the flames produced by the bronze burner. A wide range of flame conditions are studied in terms both of equivalence ratio and of gas mixture flow rate. As mentioned, all three stainless steel burners give similar soot distributions. The measured soot profiles are slightly asymmetrical, depending on the relative orientation of the burner and of the laser beam used for diagnostics. This orientation cannot be easily adjusted. Therefore, in this work, results obtained in only one new burner made of stainless steel will be presented, together with the results of the bronze one, for comparison.

Table 1
List of the investigated flames

Flame	C_2H_4 (mg/s)	Air (mg/s)	Total flow rate (mg/s)	C/O	ϕ
1	23.40	124.80	148.20	0.92	2.76
2	22.17	156.00	178.17	0.7	2.1
3	24.25	153.85	178.10	0.78	2.34
4	28.06	149.82	177.88	0.92	2.76

2. Experimental setup

Atmospheric-pressure laminar premixed ethylene/air flames as produced by McKenna burners (Holthuis & Associated, Sebastopol, CA) are studied. The main body of the burner consists of a water-cooled porous plug of 60 mm diameter. Two kinds of burner main body, stainless steel and bronze, are tested. To shield the flame from the surrounding air, an external shroud of nitrogen, flowing at 15 L/min (310 mg/s), is used. Moreover, for flame stabilization, a stainless steel plate of diameter 60 mm is placed 20 mm above the burner mouth. The flames investigated are reported in Table 1. Flame 1 has been studied extensively in our laboratory in the frame of other projects, while the other three cover a wide range of equivalence ratios ϕ with the same total flow rate, as required for the stability condition and soot detection limit. The flames 1 and 4 make it possible to test the influence of the gas flow rate at a fixed ϕ.

Mass-flow meters (Bronkhorst, AK Ruurlo, the Netherlands) are used for controlling the flows of ethylene, air, and nitrogen. The burner is placed on a motorized XYZ table to investigate the flame both in the axial and in the radial direction.

Different optical techniques including extinction, line imaging of the Rayleigh scattering, laser-induced incandescence (LII), and laser-induced fluorescence (LIF) are implemented. In the following, only a few words are spent on describing the experimental setup; more details about the techniques can be found in the references [19–28].

2.1. Extinction

For extinction measurements, the red line ($\lambda = 647$ nm) of an Ar^+Kr^+ laser (Coherent Innova 70C) is mildly focused ($1/e$ laser beam diameter of about 300 μm) into the flame and the transmitted radiation is collected, by means of a two-lens system, at the entrance of a small integrating sphere and measured

with a photosensor (Hamamatsu H5783-01). This collecting apparatus makes it possible to avoid beam steering due to thermal gradients at the flame edges. The signal is processed by a digital lock-in amplifier (Stanford, Model SR850 DSP) triggered by a mechanical chopper to discriminate against flame emission. The acquisition is driven by a personal computer. Each signal results from an average over 300 samples.

2.2. Scattering line-imaging

As for line imaging of the scattering, two lines of the same Ar^+Kr^+ laser (514 and 647 nm) are separately sent across the flame. The resulting scattered radiation, in the form of a picture of the flame crossed by the laser beam, is collected using an appropriate optical system. This apparatus consists of a cassegrain objective (Nikon, 500 mm focal length), used to avoid chromatic effects, and a CCD camera (PCO pixelfly, 12-bit) driven by a PC. Two interferential filters (514 nm, $\Delta\lambda = 9$ nm, and 647 nm, $\Delta\lambda = 10$ nm) placed just in front of the CCD camera are used for the two laser wavelengths. The collected images are processed by Image Pro Plus and MATHCAD software as described in Section 3.2.

2.3. Laser-induced incandescence

Laser-induced incandescence is performed using the fundamental beam (1064 nm, 7 ns FWHM) of a Nd:YAG laser (Quanta System, SYL 202) operating at 6 Hz. The laser beam is steered onto a diaphragm (aperture 3 mm) selecting a portion of nearly homogeneous light distribution. The diaphragm aperture is imaged on the flame axis, using a lens ($f = 285.7$ mm, $\varnothing = 70$ mm) with a magnification of 1. Efforts are spent to obtain a quite uniform-intensity cross section with sharp edges in the probe volume, as verified with a camera [26,27,29]. The incandescence signal is collected and focused, using a system of two spherical mirrors, onto the entrance slit (height 2 mm) of a monochromator (Jobin Yvon H20) coupled with a photomultiplier (Hamamatsu R955, 1.5-ns rise time). The mirrors make it possible to overcome the limitation resulting from imperfect achromaticity of commercial lenses. The two-mirror system is positioned at 30° with respect to the incident laser beam direction, to increase the probe volume and, consequently, the incandescence signal. The alignment of the receiving optics and the laser beam cross section makes it possible to obtain a probe volume with good tradeoff between signal sensitivity and spatial resolution. The incandescence signal time decay is detected with a fast digital oscilloscope (Tektronix, 1 GHz, 5 Gs/s), optically triggered by the laser shot. The detection window of the monochromator is set at 450 nm. The signal is stored in a PC and processed with a MATHCAD program. For this kind of measurement no absolute calibration procedure is performed.

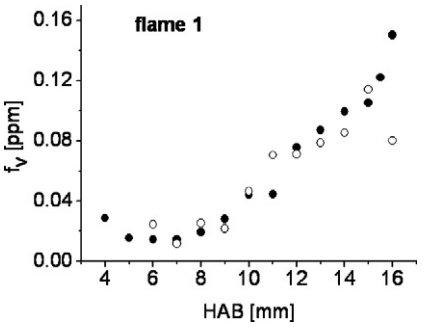

Fig. 1. Axial profile of soot volume fraction (flame 1, $\phi = 2.76$). The two symbols (open and closed) refer to measurements carried out in different days.

2.4. Laser-induced fluorescence vs scattering

Finally, in order to distinguish the contribution of fluorescent species from the scattering signal, a laser-induced fluorescence (LIF) detection apparatus is also set up by using three excitation wavelengths (488, 514, and 647 nm) of the Ar^+Kr^+ laser. The resulting signal is focused by a lens ($f = 150$ mm) onto a quartz optical fiber and sent to the entrance slit of a spectrograph (JY UFS 200, with reciprocal linear dispersion of 24 nm/mm) matched with an intensified diode array (Tracor Northern TN-1710). The overall spectral resolution was 6.25 nm. A polarizer is placed directly in front of the optical fiber to select the polarized components of the emitted radiation.

3. Measurements on the stainless steel burner, results, and discussion

3.1. Extinction

Fig. 1 shows an axial profile of the soot volume fraction, f_v, of flame 1, as obtained by extinction measurements and utilizing the refractive index of Ref. [30]. Similar trends are exhibited by the other flames. The results are obtained by considering the line-of-sight measurements of the transmitted intensity of the laser across the flame, ratioed to the length of the pathway of the laser in the flame, which in turn was measured by the imaging of the light scattering. The average value of the extinction coefficient and, consequently, of f_v can be derived. This is true in the

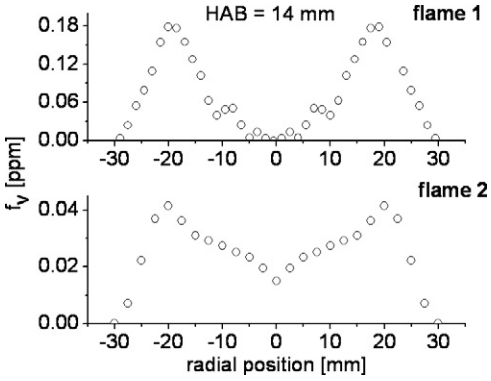

Fig. 2. Soot volume fraction radial profiles in flame 1 (top) and flame 2 (bottom) at HAB = 14 mm.

case of uniform radial distribution of soot across the flame. To verify this lateral profiles of extinction measurements are also taken. Assuming axial-symmetric geometry of the flame, lateral line-of-sight measurements are symmetrized and processed with an Abel inversion procedure in order to derive the local values of the extinction coefficient [31]. Fig. 2 shows radial profiles of f_v for flames 1 and 2 at height 14 mm above the burner. The flames considered here encompass the entire range of equivalence ratio and the flow rates investigated; therefore the following considerations can be also extended to the "intermediate" cases. Both flames show radial profiles of soot volume fraction very far from being uniform: high values of f_v are observed in an external annular region, with a minimum in the inner part of the flame. The observed behavior is more evident for flame 1, where no soot concentration is measured on the axis. Therefore, at least for these flames, it is inferred that the average value of the extinction coefficient cannot be used to evaluate the value of f_v on the axis.

The influence of the flame stabilization tools on the structure of the soot distribution is also investigated. Some tests are carried out using different stabilization devices: two plates of diameter 60 and 63 mm and different thickness were used, as well as a system composed of a 60-mm plate with a central hole for the introduction of an oil-cooled probe. This last device is generally used when sampling for gravimetric and GC analysis [12,14]. The results, not reported here, proved that the "anomalous" radial soot distribution observed cannot be attributed to a particular shape of the stabilizing plate.

3.2. Scattering

As described in the experimental section, scattering measurements are carried out in the green and red spectral regions. It is well known that the scattering signal depends on the sixth power of the soot particle diameter, d_p, and it allows, in conjunction with extinction (which depends on d_p^3), to derive the particle size. As discussed in the following, this signal can provide information about the soot distribution [32]. Fig. 3 shows a typical image collected with the CCD camera, where the scattering signal from the laser at 514 nm is superimposed on the emission radiation from the flame. The image of the scattering, as well as the emission signal, shows a very evident nonuniform structure with high-intensity regions, one stronger than the other, at each side of the flame. This effect is well visible in spite of the fact that 514 nm is not the best wavelength for this application, as will be discussed further on. In order to obtain scattering profiles from images such as the one in Fig. 3, a proper processing procedure is applied. Two sets of 10 images, one with and the other without the laser, are collected to increase the signal-to-noise ratio. Each set is processed by a MATHCAD program: after a symmetrization routine, averaged pictures are built, which are then subtracted to derive the image of the scattering. The scattering radial profile at a given height above the burner is obtained by vertical binning of six pixels. Measurements are performed at different heights above the burner. In Fig. 4, profiles at 514 nm (top) and 647 nm (bottom) are presented for flame 1. While for the case of $\lambda_{scatt} = 514$ nm profiles from 8 to 15 mm are shown, scattering signals cannot be detected with the red line below 12 mm with our laser, due to a lower scattering cross section. Profiles at greater heights were not taken because of potential interferences between the wings of the laser beam, the stabilizing plate, and soot deposited onto it. The features of the curves are quite different. In particular, at 647 nm, moving up in the flame, the profiles show the same structure, with two external peaks and a minimum in the center. On the contrary, for 514 nm, all curves are quite flat across the flame, with small peaks only at the greatest height (HAB = 15 mm). This difference is more evident by directly comparing the profiles corresponding to the same height for the two sets of measurements. For example, at HAB = 15 mm, the ratio between the peak and the minimum is 0.75 with the green line and 0.39 with the red one. From this observation, two considerations can be made: the radial nonuniformity is confirmed, and different species are responsible for the signals generated by the two wavelengths, as discussed in Section 3.4.

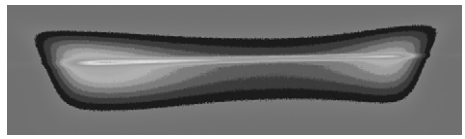

Fig. 3. Picture of the typical flame emission plus the scattering signal of the laser beam crossing the flame at 514 nm.

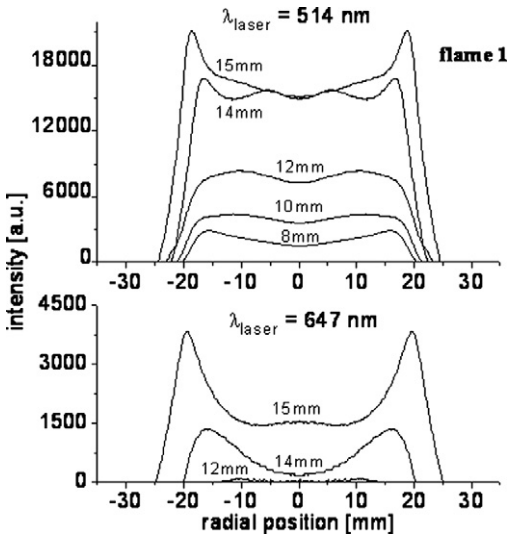

Fig. 4. Scattering line-imaging signals as a function of the height above the burner, as obtained for $\lambda_{scatt} = 514$ nm (top) and 647 nm (bottom).

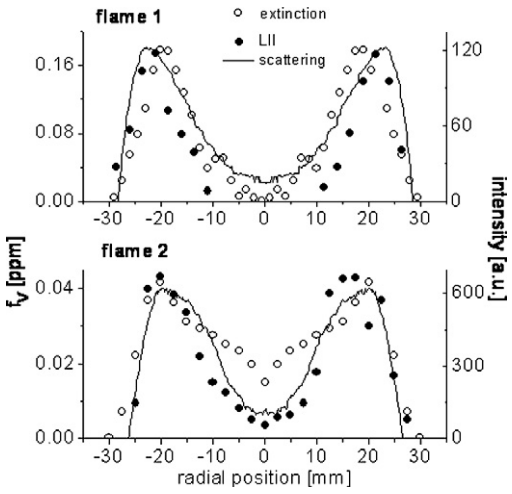

Fig. 5. Radial profiles of f_v in a stainless steel burner with the extinction measurements (open circle) and the incandescence signal (closed circle) properly scaled. Scattering profile under the same conditions (HAB = 14 mm) is shown. Results refer to flame 1 (top) and flame 2 (bottom).

3.3. Laser-induced incandescence

The laser-induced incandescence technique was performed as widely described in previous works [26,27]. The incandescence signal time decay is recorded by taking the average over 300 individual LII curves. The "prompt" signal is evaluated with integration over a 4-ns gate width around the peak (1 ns before and 3 ns after). This signal is known to be proportional to the soot volume fraction [23]. Measurements are carried out using a laser fluence of 495 mJ/cm^2, which ensures that they fall above the threshold limit, in the plateau region, with a constant soot temperature of about 4000 K in the probe volume [26,27]. In the present work no calibration procedure is performed and the incandescence signal is scaled with the soot volume fraction measurements obtained with the extinction technique. LII radial profiles (closed symbol) for flames 1 and 2 at height 14 mm above the burner are shown in Fig. 5, together with the extinction measurements (on the left y axis, open symbol) and the scattering profiles at 647 nm (right y axis, solid line). Raw data are considered for LII, without any symmetrization or other processing routine. The curves in the two sets are quite overlapped, especially in the case of flame 1. The slight discrepancy observed in the central part of flame 2 is mainly due to the mathematical inversion procedure for extinction. Since the incandescence technique is local, very sensitive, free of any processing, and related only to carbonaceous particle detection, this ensures that the flame structure observed is reliable, confirming the same soot distribution obtained with the classical but more elaborated extinction measurements. Similar behavior is exhibited by the line imaging of the scattered intensity at 647 nm, whose radial profiles are also superimposed (in arbitrary units) on the same graph (solid line). There are slight discrepancies between the profiles, such as a shift between the peaks and a different peak-to-minimum ratio. These differences can be due to different time averaging of the measurements and also may arise from the fact that LII, extinction, and scattering techniques depend differently on soot parameters. In any case, all three techniques show that the soot distribution is far from being flat. It is important to point out that the ratio of scattering and extinction measurements is related to soot particle diameter. If this ratio is almost constant, it means that the particle size is almost constant as well and, therefore, the scattering intensity can be utilized, with some caution, for the line visualization of the soot volume fraction distribution. In Ref. [24], Bengtsson and Aldén show one-dimensional images of a nearly flat soot distribution in an ethene/oxygen/nitrogen flame produced by a stainless steel McKenna burner. The measurements were obtained with laser-induced fluorescence of C_2 from laser-vaporized soot (LIF(C2)LVS) and with 50-ns time-delayed laser-induced incandescence. Both experiments used a tunable laser at 563.4 nm for excitation and a bandpass filter at 514 nm coupled with a diode array detector with a minimum gate of 100 ns for detection. This flat distribution, in contrast with our finding, could in principle be due to different burner construction or to other experimental differences (such as flame equivalence ratio, not indicated

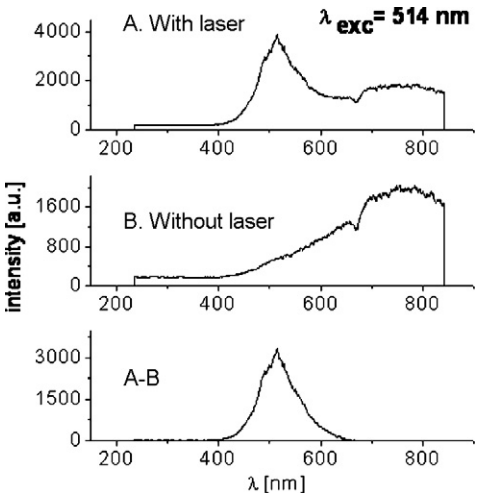

Fig. 6. Laser-induced fluorescence measurement (A–B) excited by $\lambda = 514$ nm, obtained from the difference between the total signal emitted from the flame in the presence of the laser (A) and the contribution due to the flame emission (B).

in Ref. [24]) difficult to investigate at this point. However, comparison of these results could indicate that different versions of the McKenna burner can produce different soot distributions.

3.4. Laser-induced fluorescence

The contribution of "nonsolid" species to the scattering signal was evaluated at three different excitation wavelengths, λ_{exc}. In Fig. 6, typical emission signals are shown for the case of $\lambda_{exc} = 514$ nm for a VV polarization arrangement. The bottom panel (A–B) represents the fluorescence spectrum collected on the flame axis at HAB = 14 mm. This signal results from the difference between the light intensity observed in the presence of the laser (A) and the flame emission (B). The experimental arrangement enhances the scattering, but the fluorescence signal is nevertheless strong and presents a wide unstructured band, with contributions of Stokes and anti-Stokes bands around the excitation line at 514 nm. Broadband fluorescence spectra excited by an Ar^+ laser were similarly observed in rich flames [20,33], and a LIF signal, attributed to polycyclic aromatic hydrocarbons, PAHs, was also detected with pulsed laser excitation at 563.4 nm [24].

Fluorescence spectra, as obtained with the three excitation wavelengths, are reported in Fig. 7. The spectra at $\lambda_{exc} = 488$ and 514 nm present a similar band shape, centered on the related excitation wavelength. In both cases, the contribution of the laser scattering, corresponding to the small peak at the laser wavelength in each spectrum, can be considered quite negligible with respect to the fluorescence contribution. Just to give an idea of the spectral width used, a typical laser line at 514 nm is reported in Fig. 7. Different behavior is exhibited by the signal for $\lambda_{exc} = 647$ nm, where no fluorescence band is observed. Therefore, the scattering signal in the red region can be considered almost free from any fluorescence contribution, and consequently it is related only to solid, mature soot particles. Notice the very small signal residue at the laser wavelength, due to scattering. In contrast, for the other excitation wavelengths, the fluorescence signal is very significant compared to the laser scattering. In other words, in these last cases, the total, elastic and inelastic, scattering signal measured on the flame axis (see Fig. 4) is due to the emission from solid and nonsolid species. As a further analysis, the behavior of the 514 nm excited fluorescence signal is investigated, moving vertically in the flame. To this purpose, the same heights above the burner as in the scattering line-imaging measurements are considered, and the relative spectra are shown in Fig. 8. The spectra are very similar, with increasing intensity with the height, showing that the contribution of fluorescence from "nonsolid" species is important along the flame axis.

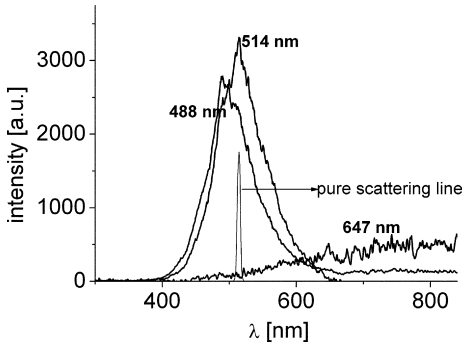

Fig. 7. Laser fluorescence spectra relative to the excitation at wavelengths 488, 514, and 647 nm. A typical laser line at 514 nm is shown.

Comparing the results from the different techniques employed, a quite complex structure of the soot distribution in the stainless steel McKenna burner is revealed. In particular, the presence of species that do not absorb in the red region but scatter/fluoresce in the visible has been observed. It is important to emphasize that, performing scattering measurements from soot, particular care in the choice of the scattering wavelength has to be taken, because the signal at 514 nm is not related only to soot. This wavelength is often used in the literature and, even when some correction is carried out in order to take into account the contribution to the scattering from fluorescing species, this procedure is at least questionable.

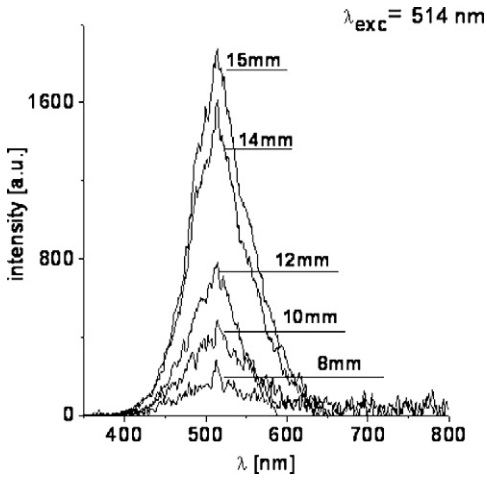

Fig. 8. Behavior of the fluorescence signal spectra moving vertically in the flame. Measurements refer to the excitation at 514 nm.

D'Alessio and co-workers studied the formation of nanoparticles of organic carbon (NOC) with optical and sampling techniques [34–36]. Their work shows that NOC are initially transparent to visible light and can only be detected with UV excitation and fluorescence [35]. In our work, nonsoot particles present in the core of rich flames produced by the stainless steel burner have been revealed, with strong fluorescence spectra excited in the visible. It will be interesting to investigate the nature of these fluorescent species.

4. Measurements on the bronze burner and comparison with the stainless steel one

In order to obtain information on the flame structure produced with the bronze burner, line-scattering measurements at 647 nm are carried out for all flames at different HAB. As an example, Fig. 9 shows the scattering profile at 14 mm, in arbitrary units, superimposed on the soot volume fraction profile obtained by extinction at the same height. Similar behavior is exhibited at other heights. Because of the different dependence on soot particle size, scattering and extinction measurements cannot be exactly compared, as previously recalled. In any case, Fig. 9 shows that with a bronze porous disk, soot is concentrated in the central part of the rich premixed flame. The decrease of f_v toward the borders is due to the nitrogen shield, which dilutes and cools the flame. This distribution is completely different from the one observed in Fig. 5 and can be considered as more resembling the flat distribution expected according to the manufacturer's design. Fig. 10 shows a comparison between flames of identical equivalence ratio, $\phi = 2.76$, but with different flow rates produced by bronze and stainless steel

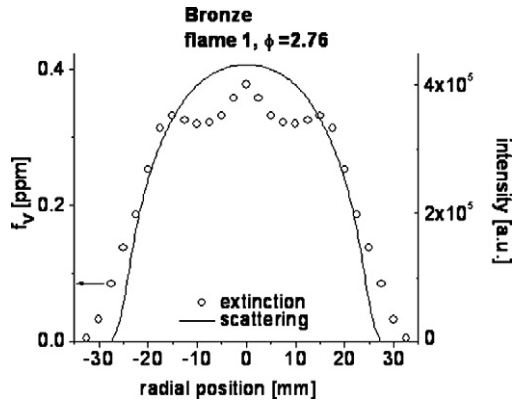

Fig. 9. Comparison of line scattering profile and f_v by extinction measurements in flame 1, produced by the bronze burner (HAB = 14 mm).

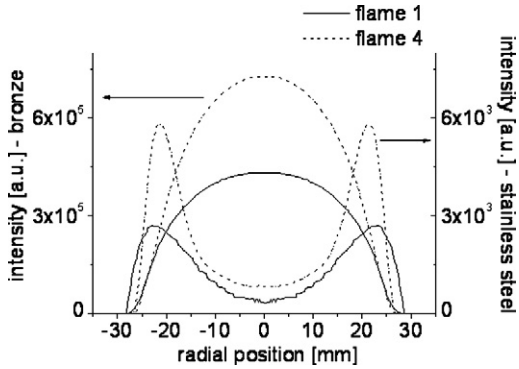

Fig. 10. Comparison of the line-scattering profiles for flame 1 and 4 produced by stainless steel and bronze burners.

plugs. The bronze configuration seems to work properly, while the stainless steel one always produces an annular soot distribution.

As already described, the soot volume fraction profiles result from mathematical processing, where a symmetrization procedure is performed and any slight nonuniformity can be masked. An analysis of the raw images related to the line scattering with the bronze plug is carried out to inspect if the soot distribution can be considered axial symmetric. Fig. 11 shows the images of flames 1 and 4 (same as Fig. 10) in gray levels chosen in order to enhance the discrepancies. Flame 4 shows an almost symmetric structure with a maximum of the emission intensity in the center of the flame due to the line-of-sight measurements. This is consistent with the flat behavior of the scattering. Similar results are obtained also for flames 2 and 3 (not reported here). A dissymmetry in the total intensity is evident for flame 1, probably due to a critical stability condition of the flame with a lower gas flow rate.

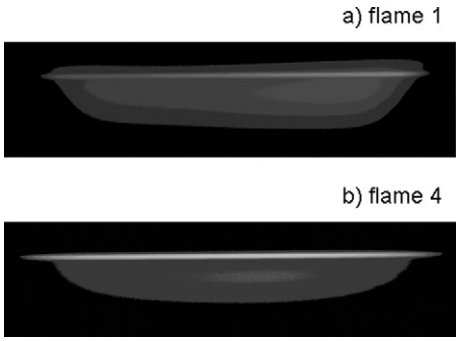

Fig. 11. Images of flame and line scattering for flame conditions 1 and 4 produced by the bronze burner.

Table 2
Integrated soot fraction at 14-mm HAB

Flame	Stainless steel (ppm cm^2)	Bronze (ppm cm^2)
1 ($\phi = 2.76$)	1.955	6.457
2 ($\phi = 2.1$)	0.632	1.868

In order to understand if, for the two burners, the different structures correspond to a different soot amount, or, conversely, if the same soot load is differently distributed at a given flame section, the integrated soot fraction over a section, $F_v(z)$, at a certain height, z, is considered. With $f_v(r, z)$ being the local value of the soot volume fraction, the integrated value can be derived as follows [25,37,38]:

$$F_v(z) = 2\pi \int_0^R f_v(r, z) r\, dr = \pi R^2 \overline{f_v(z)}. \quad (1)$$

The integrated soot fraction is expressed in ppm cm^2 and reported in Table 2 at HAB = 14 mm for flames 1 and 2, obtained with the stainless steel and bronze plugs.

As expected, an increase of F_v with ϕ is observed for both burners. Results obtained with the bronze plug are considerably higher than in the other case (more than a factor of 3). This finding is also evident by comparing the absolute values of Figs. 9 and 5 (flame 1). This consideration, together with the hollow f_v structure of the radial distribution previously shown, makes it possible to infer that any effect due to external perturbations, such as influence of the stabilizing plate or air entrainment across the nitrogen shield, can be neglected. In contrast, as the burner main body consists of a porous plug with a helical shape cooling system embedded therein, the differences could be related to the burner material and to the cooling system.

Some tests on the velocity field of the fresh gas mixture just above the burner mouth are performed with the stainless steel plug. These measurements (not reported here) are carried out using a hot-wire anemometer. Moving the burner in the XY directions, the entire cross section at HAB = 7 mm is checked, resulting in no significant variations across the flow field.

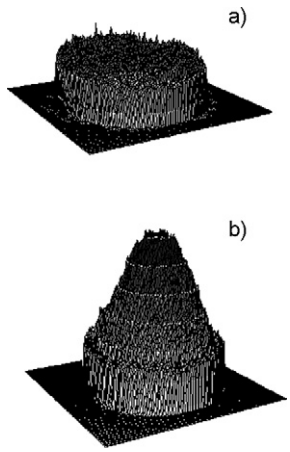

Fig. 12. Temperature mapping of burner mouth after flame switch off for bronze (a) and stainless steel (b) porous plugs. The total temperature change is on the order of 10 K.

As for the cooling, an important aspect could be the uniformity of the tubing distribution with respect to the burner mouth, which cannot be checked. Moreover, the tubing material can also play a role. In fact, while for the bronze plug the coil is copper-made, for the other burner the same stainless steel material is used. Consequently, with the thermal conductibility being very different for the two cases, both across the plug and from plug to tubing, a thermal effect can not be discarded.

The temperature distribution across the burner surface is considered by using an infrared thermo camera (Inframetric 760 E). The experimental procedure adopted to detect the burner surface temperature was the following. The flame is kept on for about 30 min for stabilization, and then it is switched off and the stabilizing plate is swung off as well. Thermal pictures of the burner surface are immediately collected. As no exact calibration for the burner material (bronze or stainless steel) could be performed, no scale is reported for the measurements. Nevertheless, since the detector was previously calibrated for iron, the variation across the burner surface can be appreciated. Fig. 12 shows the results for the bronze burner surface (a) and the stainless steel one (b). While the mapping for bronze is almost uniform, a variation of the temperature of about 10 K outlining a bell-like shape is found for stainless steel. This axial symmetric structure could be correlated with the annular soot distribution, although the small difference in the in-

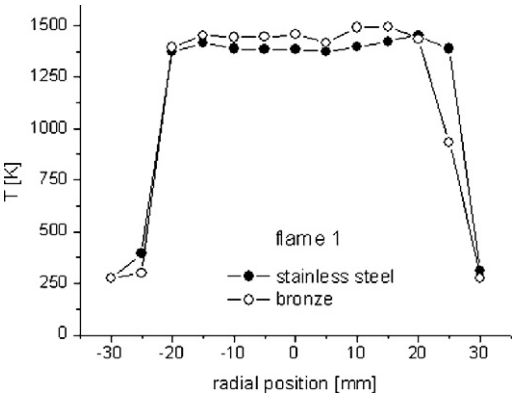

Fig. 13. Temperature profiles with flame on and thermocouple at HAB = 3 mm for the two types of burner.

let temperature of the reactants does not justify the strong variation in the soot profile. An even more surprising result comes from flame temperature measurements carried out by a radiation-corrected thermocouple (Pt/Pt–Rh(10%), 127 μm) close to the porous plug surface. The results for both types of plug are reported in Fig. 13, for HAB = 3 mm. The two profiles are quite similar and almost flat. Then, from the one hand, an undeniable difference in soot distribution obtained with the two porous plugs exists, and on the other hand, this effect occurs even though geometry, flow rates, temperatures, and flow fields can hardly account for it. It must be concluded that the combustion system here considered is not as simple as it might appear and that it should be further and thoroughly investigated both experimentally and from model calculations, taking into account minor effects.

5. Conclusions

The surprising results described in this work lead to the following conclusions.

(1) Although fed by the same ethylene and air flow rates, McKenna burners with a stainless steel or bronze porous plug produce different flames both in soot distribution and in absolute values of f_v.
(2) Rich premixed ethylene–air flames produced with a stainless steel porous disk exhibit an annular soot distribution. In the core of these flames, nonsoot fluorescing species are present.
(3) The use of short-wavelength visible laser light for soot measurements by extinction and scattering techniques in rich premixed flames can result in significant errors due to the presence of fluorescing species.
(4) Studies of soot formation mechanisms in rich premixed flames must be conducted preferentially in McKenna burners with a bronze porous disk. In general, it is suggested that researchers verify the "flatness" of the flames investigated.
(5) The differences in soot distribution observed using the stainless steel versus the bronze porous disk in flames with the same input stoichiometries, flow rates, and geometry suggest that minor effects or usually unconsidered parameters might need to be taken into account in studying soot formation mechanisms.

The authors hope that this work will help in clarifying the role that different versions of the McKenna burner can have in the determination of a standard burner for the combustion community. Researchers are advised to describe in detail the experimental conditions utilized for their investigations.

References

[1] D.W. Senser, J.S. Morse, V.A. Cundy, Rev. Sci. Instrum. 56 (6) (1985) 1279–1284.
[2] W. Clauss, V.I. Fabelinsky, D.N. Kozlov, V.V. Smirov, O.M. Stelmakh, K.A. Vereschagin, Appl. Phys. B 70 (2000) 127–131.
[3] S. Cheskis, Prog. Energy Combust. Sci. 25 (1999) 233–252.
[4] Y.-L. Chen, J.W.L. Lewis, C. Parigger, J. Quant. Spectrosc. Radiat. Transfer 66 (2000) 41–53.
[5] R.S. Barlow, C.D. Carter, Combust. Flame 97 (1994) 261–280.
[6] W. Meier, A.O. Vyrodov, V. Bergmann, W. Stricker, Appl. Phys. B 63 (1996) 79–90.
[7] S. Prucker, W. Meier, W. Stricker, Rev. Sci. Instrum. 65 (9) (1994) 2908–2911.
[8] G. Sutton, A. Levick, G. Edwards, D. Greenhalgh, Combust. Flame 147 (2006) 39–48.
[9] A. D'Alessio, G. Gambi, P. Minutolo, S. Russo, A. D'Anna, Proc. Combust. Inst. 25 (1994) 645–651.
[10] F. Xu, P.B. Sunderland, G.M. Faeth, Combust. Flame 108 (1997) 471–493.
[11] F. Xu, K.-C. Lin, G.M. Faeth, Combust. Flame 115 (1998) 195–209.
[12] A. Tregrossi, A. Ciajolo, R. Barbella, Combust. Flame 117 (1999) 553–561.
[13] B. Atakan, A. Lamprecht, K. Kohse-Höinghaus, Combust. Flame 133 (2003) 431–440.
[14] B. Apicella, M. Alfè, R. Barbella, A. Tregrossi, A. Ciajolo, Carbon 42 (2004) 1583–1589.
[15] A.V. Menon, S.-Y. Lee, M.J. Linevsky, T.A. Litzinger, R.J. Santoro, Proc. Combust. Inst. 31 (2007) 593–601.
[16] B. Axelsson, R. Collin, P.-E. Bengtsson, Appl. Opt. 39 (21) (2000) 3683–3690.
[17] V. Kruger, C. Wahl, R. Hadef, K.P. Geigle, W. Stricker, M. Aigner, Meas. Sci. Technol. 16 (2005) 1477–1486.
[18] C. Schulz, B.F. Kock, M. Hoffmann, H. Michelsen, S. Will, B. Bougie, R. Suntz, G. Smallwood, Appl. Phys. B 83 (2006) 333–354.

[19] A. D'Alessio, A. Di Lorenzo, A. Borghese, F. Beretta, S. Masi, Proc. Combust. Inst. 16 (1977) 695–708.
[20] B.S. Haynes, H. Jander, H.Gg. Wagner, Ber. Bunsenges. Phys. Chem. 84 (1980) 585–592.
[21] S.J. Harris, A.M. Weiner, Combust. Sci. Technol. 31 (1983) 155–167.
[22] W.L. Flower, Combust. Sci. Technol. 33 (1983) 17–33.
[23] L.A. Melton, Appl. Opt. 23 (1984) 2201–2208.
[24] P.-E. Bengtsson, M. Aldén, Appl. Phys. B 60 (1995) 51–59.
[25] F. Cignoli, S. De Iuliis, G. Zizak, Fuel 80 (2001) 945–955.
[26] S. De Iuliis, F. Cignoli, G. Zizak, Appl. Opt. 44 (34) (2005) 7414–7423.
[27] S. De Iuliis, F. Migliorini, F. Cignoli, G. Zizak, Appl. Phys. B 83 (2006) 397–402.
[28] K. Kohse-Höinghaus, J.B. Jeffries (Eds.), Applied Combustion Diagnostics, Taylor & Francis, New York, 2002.
[29] F. Cignoli, S. De Iuliis, G. Zizak, Appl. Spectrosc. 58 (11) (2004) 1372–1375.
[30] H. Chang, T.T. Charalampopoulos, Proc. R. Soc. London Ser. A 430 (1990) 577–591.
[31] C.J. Dasch, Appl. Opt. 31 (1992) 1146–1152.
[32] C.J. Dasch, D.M. Heffelinger, Combust. Flame 85 (1991) 389–402.
[33] P. Minutolo, G. Gambi, A. D'Alessio, A. D'Anna, Combust. Sci. Technol. 101 (1994) 311–325.
[34] P. Minutolo, G. Gambi, A. D'Alessio, S. Carlucci, Atmos. Environ. 33 (1999) 2725–2732.
[35] L.A. Sgro, P. Minutolo, G. Basile, A. D'Alessio, Chemosphere 42 (2001) 671–680.
[36] L.A. Sgro, G. Basile, A.C. Barone, A. D'Anna, P. Minutolo, A. Borghese, A. D'Alessio, Chemosphere 51 (2003) 1079–1090.
[37] R.J. Santoro, T.J. Yeh, J.J. Horvath, H.G. Semerjian, Combust. Sci. Technol. 53 (1987) 89–115.
[38] R. Villasenor, I.M. Kennedy, Proc. Combust. Inst. 24 (1992) 1023–1030.